confirm the strong polarisation suppression of ~30 dB within the singlemode operation regime of device 5_90.

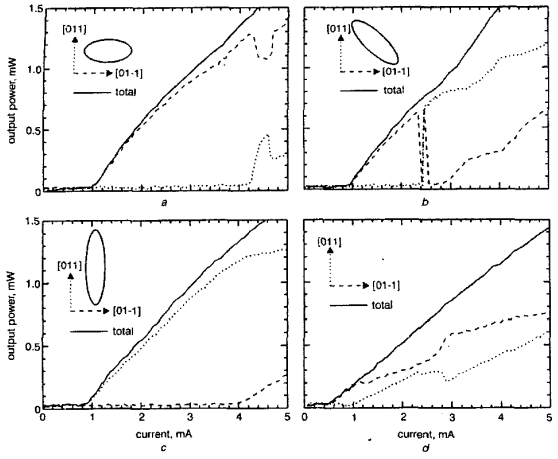

Fig. 1 *Polarisation-resolved LIV-characteristics of four differently etched 5 μm aperture diameter devices*

Insets: orientation and aspect ratio of etched ellipses
a 5_90
b 5_45
c 5_0
d 5_U

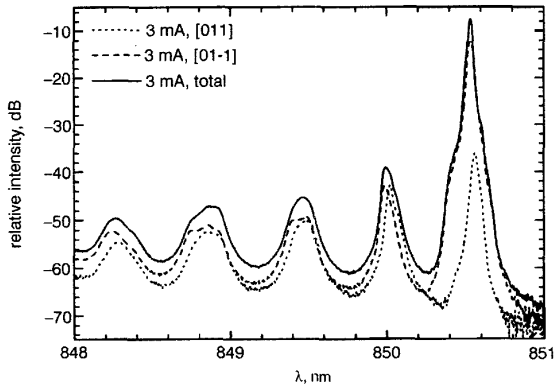

Fig. 2 *Polarisation-resolved spectra of device 5_90*

The spectral behaviour of device 5_90 at a current of 10 mA, well into the multimode regime, is shown in Fig. 3. Even though higher-order modes contain various fractions of both polarisations, the fundamental mode polarisation is still pinned to the [01$\bar{1}$] crystal direction with a similar suppression ratio as before. This indicates that the polarisation selection mechanism may be strong enough for applications such as high-speed data transmission.

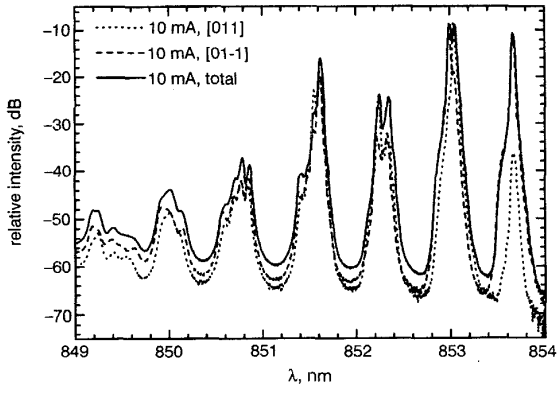

Fig. 3 *Polarisation-resolved spectra of device 5_90*

Conclusion: We have successfully fabricated for the first time 850 nm selectively oxidised VCSELs with a self-aligned elliptical shallow surface relief. Continuous-wave measurements at room temperature with the bare die sample held by vacuum on a copper block have been carried out on a large number of devices. These measurements show deterministic polarisation selection of the fundamental mode with ~30 dB suppression ratio over the complete operating range if the ellipse is aligned along the [011] or [01$\bar{1}$] crystal axis. By using a layer structure with lower *p*-side reflectivity in the future, we expect to greatly augment the effect, resulting in a much higher singlemode, single-polarisation current range and optical output power. In addition, the strength of the polarisation pinning will be evaluated by applying mechanical strain, elevated temperatures and high-speed modulation.

Acknowledgment: This work is supported by the German Ministry for Research and Technology (BMBF). We wish to thank G. Steinle at Infineon Technologies, Munich, for providing the epitaxial material.

19 October 2001
Electronics Letters Online No: 20020040
DOI: 10.1049/el:20020040

H.J. Unold, M.C. Riedl, R. Michalzik and K.J. Ebeling (*University of Ulm, Department of Optoelectronics, D-89069 Ulm, Germany*)

E-mail: heiko.unold@e-technik.uni-ulm.de

K.J. Ebeling: Also at Infineon Technologies, Munich, Germany

References

1 PANAJOTOV, K., DANCKAERT, J., VERSCHAFFELT, G., PEETERS, M., NAGLER, B., ALBERT, B., RYVKIN, B., THIENPONT, H., and VERETENNICOFF, I.: 'Polarization behavior of vertical-cavity surface-emitting lasers: experiments, models and applications', *Nanoscale and Nonlinear Optics: International School on Quantum Electronics, Proc. AIP*, 2001, **560**, pp. 403–417

2 WEIGL, B., GRABHERR, M., JUNG, C., JÄGER, R., REINER, G., MICHALZIK, R., SOWADA, D., and EBELING, K.J.: 'High-performance oxide-confined GaAs VCSELs', *IEEE J. Sel. Top. Quantum Electron.*, 1997, **3**, (2), pp. 409–415

3 KANEKO, Y., MARS, D., NAKAGAWA, S., ICHIMURA, Y., and YAMADA, N.: 'Vertical-cavity surface-emitting lasers with stable polarization grown on (411)A-oriented substrates', *Jap. J. Appl. Phys.*, 1999, **38**, (8A), pp. 864–866

4 BERSETH, C.-A., DWIR, B., UTKE, I., PIER, H., RUDRA, A., IAKOVLEV, V.P., and KAPON, E.: 'Vertical cavity surface emitting lasers incorporating structured mirrors patterned by electron-beam lithography', *J. Vac. Sci. Technol. B*, 1999, **17**, (6), pp. 3222–3225

5 UNOLD, H.J., MAHMOUD, S.W.Z., JÄGER, R., GRABHERR, M., MICHALZIK, R., and EBELING, K.J.: 'Large-area single-mode VCSELs and the self-aligned surface relief', *J. Sel. Top. Quantum Electron.*, 2001, **7**, (2), pp. 386–392

6 UNOLD, H.J., GOLLING, M., MEDERER, F., MICHALZIK, R., SUPPER, D., and EBELING, K.J.: 'Singlemode output power enhancement of InGaAs VCSELs by reduced spatial hole burning via surface etching', *Electron. Lett.*, 2001, **37**, (9), pp. 570–571

Parallel feed travelling wave distributed *pin* photodetectors with integrated MMI couplers

S. Murthy, M.C. Wu, D. Sivco and A.Y. Cho

The fabrication and performance of a parallel feed travelling wave photodetector with *pin* diodes operating at 1550 nm is presented. A parallel optical feed using an integrated multimode interference (MMI) power splitter helps increase the maximum linear photocurrent through a more uniform distribution of photocurrent. The maximum DC linear current measured is 52.2 mA. Maximum linear RF power at 10 GHz was 9 dBm.

Introduction: High-power, high-speed photodetectors reduce RF insertion loss and increase spurious-free-dynamic-range and signal-to-noise ratio of analogue fibre optic links [1, 2]. In digital applications, high-speed, high-power detectors are important for 40 Gbit/s systems and beyond, because they enable optical pre-amplification to

increase the sensitivity of the receiver [3]. Velocity-matched distributed photodetectors (VMDP) have demonstrated high-bandwidth and high saturation current by increasing the total absorption volume while adding the electrical signal from the individual photodiodes in phase [4, 5]. In these serially-fed VMDPs, however, the device fails while still in the linear photocurrent regime due to thermal runaway of the first detector in the array [6]. This is due to the exponentially decaying distribution of photocurrents in the diodes of the series array. A uniform distribution of photocurrents will help achieve higher linear photocurrents. Parallel feed of the individual photodiodes achieves uniform photocurrent distribution. In addition, the peak photocurrent is reduced by the splitting ratio. The maximum linear photocurrent thus increases with increasing splitting ratio. Parallel feed of distributed diodes using discrete components has previously been demonstrated [7].

We have previously demonstrated the first monolithic parallel feed distributed photodetectors with integrated MMI splitters [8]. These detectors, fabricated with metal-semiconductor-metal (MSM) diodes, were limited in bandwidth by carriers generated in the low field regions. *pin* diodes have a more uniform electric field distribution in the absorption region and have been shown to operate at higher temperatures [9] before failure compared to MSM diodes [6]. This is primarily due to the higher activation energy for dark current in *pin* diodes. In this Letter, we report the experimental results of parallel feed travelling wave photodetectors with *pin* diodes. Both DC and RF linearity characteristics are measured.

Design and fabrication: The material system used for the wafer growth is the InAlGaAs system. The absorbing region is a 0.25 μm thick layer of InGaAs. The 1×4 MMI, designed using the BeamProp (BPM) method is 0.95 mm long and 40 μm wide. Each output waveguide of the splitter is 6 μm wide and the spacing between output waveguides is 4 μm. The *pin* diode itself is 80 μm long and the absorbing region is a 2 μm wide mesa. A 50 Ω velocity matched transmission line is employed to collect the signal from the four diodes in phase.

The device mesas are patterned using wet etching, and the metal patterns defined using *e*-beam evaporation followed by liftoff. A scanning electron micrograph (SEM) of the fabricated device is shown in Fig. 1. The *p*-contact is formed on a layer with low doping concentration because the etch stop layer does not have enough selectivity. The resulting *p*-contact specific resistance is $\sim 10^{-4}\ \Omega/\text{cm}^2$. The bandwidth of our detector is thus limited by the RC time constant instead of velocity mismatch.

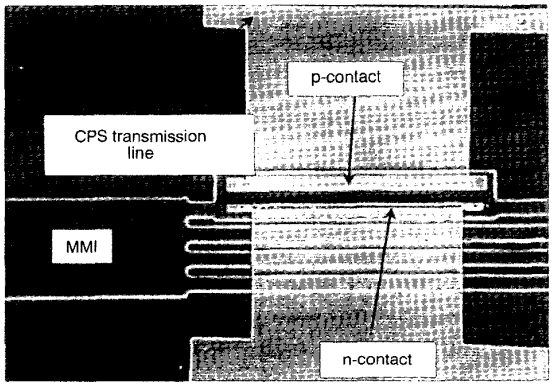

Fig. 1 *SEM of fabricated device showing 80 μm long pin diode and portions of MMI splitter and 50 Ω transmission line*

Measurement results: The DC photocurrent measurement, made by coupling light into the detector through a lensed-fibre is shown in Fig. 2. The responsivity in this measurement is 0.17 A/W. When using a fibre pickup head consisting of bulk microlenses, the detector shows a higher responsivity of 0.21 A/W. The two main loss components are the coupling efficiency into the optical waveguide and the Fresnel reflection loss at the semiconductor interface. The DC photocurrent is linear up to 52.2 mA. To our knowledge, this is the highest reported DC photocurrent for 1.55 μm detectors. This current is limited by the maximum possible output of our erbium-doped fibre amplifier (EDFA). We believe we can reach even higher linear photocurrents, either by increasing the optical input to the detector or by improving the responsivity of our detector through a spot-size converter and an anti-reflection coating.

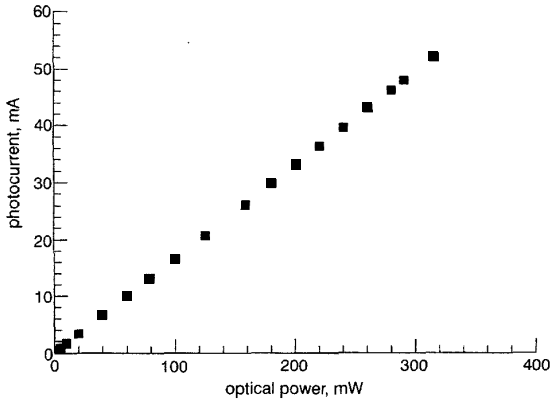

Fig. 2 *DC saturation measurement*
DC photocurrent is linear till 52.2 mA (for maximum possible output of our EDFA)

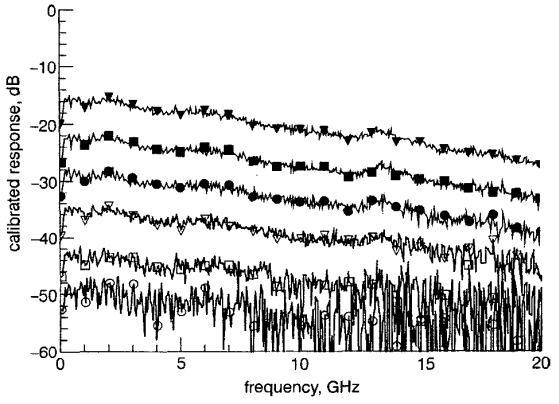

Fig. 3 *Frequency response for input optical power varying in 3 dB steps*

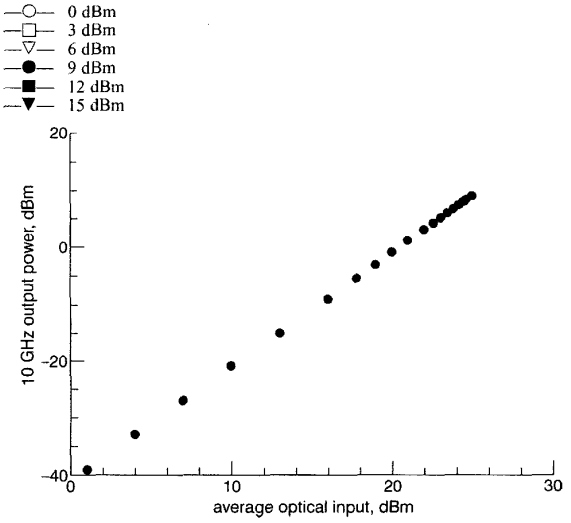

Fig. 4 *Linearity measurement of 10 GHz RF output*

The frequency response of the detector was measured using a 20 GHz HP Lightwave test set. The 3 dB bandwidth is 9 GHz for reverse bias voltages greater than 3 V. This bandwidth is limited by the ohmic contact resistance, as mentioned earlier. The frequency response is shown in Fig. 3 for various optical input power levels varying in 3 dB steps. The frequency response shows no saturation up to 15 dBm of optical input.

We have also performed an optical heterodyne experiment to measure the dependence of the generated microwave power on the input optical power. Two optical wavelengths, separated by 10 GHz, were amplified by an EDFA and then coupled to a photodetector. An optical attenuator and polarisation controllers were used to control the input optical power and the input polarisations. The generated RF signal was collected with a 40 GHz GGB Industries Picoprobe and measured using an HP8487A power sensor-power meter. The measured RF power increases quadratically with the input optical power (Fig. 4), indicating the photodetector is linear at 10 GHz for the entire optical power range. The maximum linear RF power of 9 dBm is limited by the available optical power.

Conclusion: We have successfully fabricated a parallel feed travelling wave *pin* photodetctor with an integrated 1×4 MMI power splitter. The DC photocurrent is linear till 52.2 mA, which is the highest current reported for detectors operating at 1.55 μm wavelength. The RF bandwidth measurement from 0.045–20 GHz shows no saturation for up to 15 dBm of input optical power. The optical heterodyne output of the detector is linear up to 9 dBm of 10 GHz RF power.

Acknowledgments: The authors would like to acknowledge the helpful discussions with S. Islam and T. Jung. This work was funded by DARPA as part of the COAST project.

25 October 2001
Electronics Letters Online No: 20020043
DOI: 10.1049/el:20020043

S. Murthy and M. C. Wu (*Electrical Engineering Department, University of California, Los Angeles, CA 90095, USA*)

E-mail: sanjeev@icsl.ucla.edu

D. Sivco and A. Y. Cho (*Lucent Technologies, Bell Laboratories, Murray Hill, NJ 07974, USA*)

References

1 COX, C.H.: 'Gain and noise figure in analogue fibre-optic links', *IEE Proc. J.*, 1992, **139**, (4), pp. 238–242
2 WILLIAMS, K.J., NICHOLS, L.T., and ESMAN, R.D.: 'Photodetector nonlinearity limitations on a high-dynamic range 3 GHz fiber optic link', *J. Lightwave Technol.*, 1998, **16**, (2), pp. 192–199
3 MIYAMOTO, Y., YONEYAMA, M., HAGIMOTO, K., ISHIBASHI, T., and SHIMIZU, N.: '40 Gbit/s high sensitivity optical receiver with uni-travelling-carrier photodiode acting as decision IC driver', *Electron. Lett.*, 1998, **34**, (2), pp. 214–215
4 LIN, L.-Y., WU, M.C., ITOH, T., VANG, T.A., MULLER, R.E., SIVCO, D.L., and CHO, A.Y.: 'Velocity-matched distributed photodetectors with high-saturation power and large bandwidth', *IEEE Photonics Technol. Lett.*, 1996, **8**, (10), pp. 1376–1378
5 ISLAM, M.S., JUNG, T., ITOH, T., WU, M.C., SIVCO, D., and CHO, A.Y.: 'Velocity matched distributed detectors with *pin* diodes'. Tech. Digest, MWP 2000, Oxford, UK 11–13 Sept. 2000, pp. 217–220
6 NESPOLA, A., CHAU, T., WU, M.C., SIVCO, D., and CHO, A.Y.: "Analysis of failure mechanisms in velocity-matched distributed photodetectors", *IEE Proc., Optoelectron*, 1999, **146**, (1), pp. 25–30
7 GOLDSMITH, C.L., MAGEL, G.A., and BACA, R.J.: 'Principles and performance of traveling-wave photodetector arrays', *IEEE Trans. Microw. Theory Tech.*, 1997, **45**, (8), pp. 1342–1350
8 MURTHY, S., JUNG, T., CHAU, T., WU, M.C., SIVCO, D., and CHO, A.Y.: 'A novel monolithic distributed traveling-wave photodetector with parallel optical feed', *IEEE Photonics Technol. Lett.*, 2000, **12**, (6), pp. 681–683
9 WILLIAMS, K.J., and ESMAN, R.D.: 'Design considerations of high current photodetectors', *J. Lightwave Technol.*, 1999, **17**, (8), pp. 1443–1454

OFDM-CPM signals

I.A. Tasadduq and R.K. Rao

A class of orthogonal frequency division multiplexing–continuous phase modulation (OFDM-CPM) signals is introduced in which binary data sequence is mapped to complex symbols using the concept of correlated phase states of a CPM signal. Various types of signals are defined as a function of parameter h and pulse duration. An investigation of bit error rate and peak-to-average-power ratio performance of these signals is also presented.

Introduction: Orthogonal frequency division multiplexing (OFDM) is a good candidate for wireless communication owing to its excellent properties in frequency-selective fading environments [1].

While in the literature OFDM-PSK, -QAM, -DPSK and -DAPSK have been considered [2–4], OFDM–continuous phase modulation (CPM) signals that use the concept of correlated phase states of a CPM signal have not been considered to date. One of the advantages of OFDM-CPM signals is that correlation amongst adjacent OFDM symbols can be systematically introduced by an appropriate choice of parameter h (in typical CPM signals h is modulation index). Furthermore, this correlation can be exploited to control bit error rate (BER).

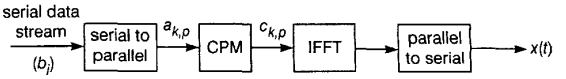

Fig. 1 *OFDM-CPM transmitter*

OFDM-CPM signalling scheme: As shown in Fig. 1, serial bit stream $b_i, i=0, 1, 2, \ldots$ with bit duration of T_b seconds is converted into blocks of N bits represented by $a_{k,p}; k=0, 1, 2, \ldots$ and $p=0, 1, 2, \ldots, N-1$, where N denotes the number of carriers and $a_{k,p}=\pm 1$, e.g. $a_{0,p}$ would denote the first block of N bits and $a_{1,p}$ the second block of N bits, and so on. The CPM mappers transform the incoming $\{a_{k,p}\}$ into appropriate complex numbers $\{c_{k,p}\}$, i.e.

$$c_{k,p} = \cos(\theta_{k,p}) + j\sin(\theta_{k,p}) \tag{1}$$

with

$$\theta_{k,p} = a_{k,p}\pi h + \pi h \sum_{q=0}^{k-1} a_{q,p} + \phi \tag{2}$$

where parameter h defines the CPM mapper and ϕ represents the initial mapping point. In (2) the angles $\theta_{k,p}$ depend not only on the current data but also on the past data. Current value of θ is determined by adding $+\pi h$ (for data $a+1$) or $-\pi h$ (for data $a-1$) to the previous value of θ. The complex numbers from the output of CPM mappers that lie on a circle are passed through pulse-shaping filters $g(t)$, modulated by orthogonal carriers and summed to give the transmitted OFDM symbol, i.e.

$$x(t) = \sum_k \sum_p c_{k,p} g(t-kT) e^{j(2\pi/T)pt}, \qquad 0 \le t < \infty \tag{3}$$

where

$$g(t) = \begin{cases} \dfrac{1}{\sqrt{T}} & 0 \le t \le LT \\ 0 & \text{elsewhere} \end{cases} \tag{4}$$

In (3), $T(=NT_b)$ is the OFDM symbol duration and in (4) $L=1$ for full response signalling. The parameters h and L can be chosen in various ways. Some of the OFDM-CPM signals are described below.

A. Single-h OFDM-CPM signals: In this case, the value of h remains constant for all OFDM symbols. By choosing h to be rational and $0<h<1$ it is possible to have a finite number of points in the CPM constellation. Fig. 2 shows the constellation diagram of CPM mapper for $h=1/2$ and $h=1/4$.

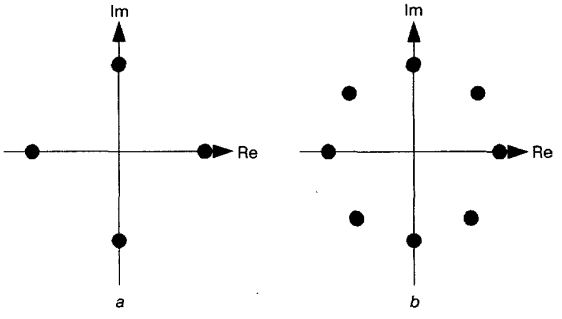

Fig. 2 *Constellation diagram of CPM mapper*
a $h=1/2$
b $h=1/4$